Electrostatic Interactions between Double Layers: Influence of Surface Roughness, Regulation, and Chemical Heterogeneities

ARTICLE *in* LANGMUIR · JULY 2004

Impact Factor: 4.46 · DOI: 10.1021/la030404f · Source: PubMed

3 AUTHORS, INCLUDING:

Jerome F.L. Duval
French National Centre for Scientific Research
111 PUBLICATIONS **1,941** CITATIONS

SEE PROFILE

Frans A M Leermakers
Wageningen University
289 PUBLICATIONS **4,755** CITATIONS

SEE PROFILE

Electrostatic Interactions between Double Layers: Influence of Surface Roughness, Regulation, and Chemical Heterogeneities

J. F. L. Duval,* F. A. M. Leermakers, and H. P. van Leeuwen

Department of Physical Chemistry and Colloid Science, Wageningen University, Dreijenplein 6, 6703 HB Wageningen, The Netherlands

Received November 4, 2003. In Final Form: February 24, 2004

Electrostatic interactions between two surfaces as measured by atomic force microscopy (AFM) are usually analyzed in terms of DLVO theory. The discrepancies often observed between the experimental and theoretical behavior are usually ascribed to the occurrence of *chemical regulation* processes and/or to the presence of *surface chemical* or *morphological heterogeneities* (roughness). In this paper, a two-gradient mean-field lattice analysis is elaborated to quantifying double layer interactions between nonplanar surfaces. It allows for the implementation of the aforementioned sources of deviation from DLVO predictions. Two types of ion−surface interaction ensure the adjustment of charges and potentials upon double layer overlap, i.e., specific ionic adsorption at the surfaces and/or the presence of charge-determining ions for the surfaces considered. Upon double layer overlap, charges and potentials are adjusted via reequilibrium of the different ion adsorption processes. Roughness is modeled by grafting asperities on supporting planar surfaces, with their respective positions, shapes, and chemical properties being assigned at will. Local potential and charge distributions are derived by numerically solving the nonlinear Poisson−Boltzmann equation under the boundary conditions imposed by the surface profiles and regulation mechanism chosen. Finite size of the ions is taken into account. A number of characteristic situations are briefly discussed. It is shown how the surface irregularities are reflected in the Gibbs energy of interaction.

1. Introduction

Accurate knowledge of the interactions between two surfaces is a mandatory prerequisite for understanding a variety of colloidal and interfacial phenomena, such as heterocoagulation, particle deposition, electrosorption, or rheological behavior. Classically, the Gibbs energy of interaction between two charged colloidal particles is described by means of the DLVO theory.[1,2] This theory is widely regarded as a cornerstone for understanding colloidal systems and forces on the molecular scale and for predicting macroscopic properties of colloidal dispersions. It reconciles long-range electrostatic double layer interaction[3,4] and short-range Lifshitz−van der Waals interaction.[5,6] The classical DLVO theory is based on the assumption that the Lifshitz−van der Waals component can be superimposed on the electrostatic contribution to the pair interaction (superposition approximation). Furthermore it is taken that the interacting surfaces are perfectly smooth and that their surface charge densities are uniform, that is, independent of position. Within these assumptions, the double layer properties are smeared-out along the surface: the potential and charge distributions develop according to one spatial variable, i.e., the dimension perpendicular to the surfaces. As such, the electrostatic part of the DLVO theory can be considered as a self-consistent field approach. However, real colloidal systems generally contain some degree of nonuniformity, in the form of surface roughness and/or chemical heterogeneities. The applicability of the DLVO theory for such systems is questionable, as indicated by various experimental data, which fail to match theoretical prediction. Representative illustrations of the inadequacy of the DLVO theory are provided by surface force/atomic force microscopy measurements,[7−9] particle deposition experiments,[10−13] and coagulation kinetics analyses.[14,15]

In an effort to account for the discrepancies between theory and experiment, many attempts were made to modify the existing theory so as to include roughness effects or chemical heterogeneities and to evaluate the corresponding van der Waals and electrostatic interactions. The current paper focuses on the importance of surface nonuniformities in determining interaction forces between two surfaces. In the framework of this context, we shall be interested in the computation of the electrostatic contribution of the total interaction curve. This latter component is sensitive to both surface roughness and chemical heterogeneities. Until now, these two types of nonuniformities have been studied independently. Stank-

* To whom correspondence may be addressed. E-mail: jerome.duval@wur.nl. Tel.: 00 31 317 484 960. Fax: 31 (0)317 483 777.

(1) Verwey, E. J. W.; Overbeek, J. Th. G. In *Theory of Stability of Lyophobic Colloids*; Elsevier: Amsterdam, 1948.
(2) Derjaguin, B. V.; Landau, L. *Acta Physicochim. URSS* **1941**, *14*, 633.
(3) Russel, W. B.; Saville, D. A.; Schowalter, W. R. In *Colloidal Dispersions*; Cambridge University Press: Cambridge, 1989.
(4) Israelachvili, J. N. In *Intermolecular and Surface Forces*, 2nd ed.; Academic Press: London, 1992.
(5) Lifshitz, E. M. *Z. Eksp. Teor. Fiz.* **1955**, *29*, 44.
(6) Hamaker, H. C. *Physica* **1937**, *4*, 1058.
(7) Tsao, Y.-H.; Yang, S. X.; Evans, D. F.; Wennerström, H. *Langmuir* **1991**, *7*, 3154.
(8) Tsao, Y.-H.; Evans, D. F.; Wennerström, H. *Science* **1993**, *262*, 547.
(9) Tsao, Y.-H.; Evans, D. F.; Wennerström, H. *Langmuir* **1993**, *9*, 779.
(10) Marshall, J. K.; Kitchener, J. A. *J. Colloid Interface. Sci.* **1966**, *22*, 342.
(11) Hull, M.; Kitchener, J. A. *Trans. Faraday. Soc.* **1969**, *65*, 3093.
(12) Elimelech, M.; Gregory, J.; Jia, X.; Williams, R. A. In *Particle Deposition and Aggregation: Measurement, Modeling and Simulation*; Butterworth: Oxford, 1995.
(13) Walz, J. *Adv. Colloid Interface Sci.* **1998**, *74*, 119.
(14) Kihira, H.; Ryde, N.; Matijevic, E. *J. Chem. Soc., Faraday. Trans.* **1992**, *88 (16)*, 2379.
(15) Vreeker, R.; Kuin, A. J.; den Boer, D. C.; Hoekstra, L. L.; Agterof, W. G. M. *J. Colloid Interface. Sci.* **1992**, *154*, 138.

10.1021/la030404f CCC: $27.50
Published on Web 05/06/2004

ovich et al.[16] analyzed the interactions between ideally spherical particles with periodic or random nonuniform surface potentials. The use of the linear Poisson−Boltzmann equation allowed the decoupling of the interactions between uniform and nonuniform components of the surface potential and the (analytical) calculation of the torque and force that particles in a doublet exert on one another. Other types of surface potential/charge distributions were investigated, and the reader is referred to the paper of Stankovich et al. where further references are given. These studies, particularly relevant in the field of heterocoagulation, focus on nonuniform surface potential and/or charge distributions for which experimental evidence is absent. In the past decade, studies of interactions between rough surfaces have become numerous. They may be classified according to the realistic character of the roughness considered. Common approaches consist of generating geometrically regular asperities,[13,17−21] either conic, hemispheric, spherical, cylindrical, or sinusoidal, on one or both surfaces. To compute the corresponding electric double layer interaction energy, solution of the Poisson−Boltzmann (PB) equation is required. It is obtained for the geometries chosen following procedures differing by their degree of mathematical sophistication. Linearization of the PB equation, application of the linear superposition theorem,[22] employment of rigorous numerical schemes such as boundary element,[23] finite element,[24,25] or finite differences[26,27] illustrate the variety of tools commonly adopted. A simple alternative is the use of the Derjaguin approximation (DA).[28,29] It relates the interaction per unit area between two flat parallel planes to the corresponding interaction between curved surfaces. This technique is known to be valid only when the principal radius of curvature of the asperities is well above the separation distance and the range of the interactions. Recent extension of the DA has been proposed by Bhattacharjee et al., under the name of surface element integration (SEI) technique.[30,31] This technique involves the integration of the corresponding interaction between two flat plates over the exact geometry of the rough surfaces. Contrary to the DA, it is capable of treating both concave and convex asperities and can be applied to very small asperities. Newly developed methods for the generation of roughness have led to a considerable breakthrough in the effort to mimic the real topology of colloids. The use of the fractal approach,[32,33] the possibility of generating asperities randomly distributed on a surface,[13,17−21,34] or matching the shape of a colloid by means of a combination of flat and triangular surface elements[35] illustrates the development toward approaching the actual form of surface roughness.

However, despite this variety of techniques and their various degrees of rigor with respect to roughness integration, all these analyses have in common that the boundary conditions adopted for solving the PB equation refer to the very restrictive constant potential or constant charge conditions. In reality, intermediate situations are more likely to occur, and this has recently been underlined for the interaction between one-dimensional (1D) double layers.[36] Besides, as already mentioned, methods that allow for the concomitant effects of chemical heterogeneities and surface roughness have not been reported so far. Of course, real surfaces will likely contain both of these nonuniformities, as the surface charge on a protrusion could be different from that of the surrounding surface. As mentioned by Walz in a review on the effects of surface heterogeneities on colloidal forces,[13] models accounting for both factors are still needed. To come closer to reality, we here propose a two-gradient mean-field lattice analysis to evaluate electrostatic interactions between regulating electric double layers at rough surfaces containing chemical heterogeneities. We are aware that commercially available programs are commonly used to solve the Poisson−Boltzmann equation in three dimensions for charged macromolecules (proteins, for example). To our knowledge, such programs are written either for single macromolecule[37] (no interaction macromolecule−macromolecule considered) or for interaction situations within the restrictive constant potential or constant charge approximations.[38] It would be pretentious and erroneous to say that the formalism presented here allows simulations of regulation processes occurring upon encounter of such complicated macrobodies. Nonetheless, its applicability for the colloid stability issue and for understanding electrostatic interactions (including regulation) between surfaces of well-defined chemical and morphological heterogeneities is new.

2. Method of Calculation

All the results presented in this paper were obtained using a computer program, called sfbox, developed on the basis of the Scheutjens−Fleer theory[39] and recently extended and generalized by Van Male.[40] Considering the wide spectrum of problems that can be dealt with (wetting phenomena, adsorption of polymers, surfactants or polyelectrolytes at interfaces), complete description of the numerical scheme in the program is beyond the scope of the current paper. Interested readers are referred to ref 40 for that purpose. Instead, we shall give a comprehensive description of the problem by first writing the basic electrostatic equations and boundary conditions in their continuous forms and then sketching the general discretization procedure adopted and its useful character for generating topologic and chemical nonuniformities at the surfaces. Transient effects will not be tackled here, only electric double layers at equilibrium are considered.

(16) Stankovich, J.; Carnie, S. L. *J. Colloid Interface. Sci.* **1999**, *216*, 329.
(17) Elimelech, M.; O'Melia, C. R. *Langmuir* **1990**, *6*, 1153.
(18) Herman, M. C.; Papadopoulos, K. D. *J. Colloid Interface. Sci.* **1990**, *136*, 385.
(19) Herman, M. C.; Papadopoulos, K. D. *J. Colloid Interface. Sci.* **1991**, *142*, 331.
(20) Suresh, L.; Walz, J. *J. Colloid Interface. Sci.* **1996**, *183*, 199.
(21) Suresh, L.; Walz, J. *J. Colloid Interface. Sci.* **1997**, *196*, 177.
(22) Sader, J. E.; Lenhoff A. M. *J. Colloid Interface. Sci.* **1998**, *201*, 233.
(23) Grant, M. L.; Saville, D. A. *J. Colloid Interface. Sci.* **1995**, *171*, 35.
(24) Chan, B. K. C.; Chan, D. Y. C. *J. Colloid Interface. Sci.* **1983**, *92*, 281.
(25) Stankovich, J.; Carnie, S. L. *Langmuir* **1996**, *12*, 1453.
(26) Hoskin, N. *Philos. Trans. R. Soc. London* **1956**, *248*, 433.
(27) Hoskin, N.; Levine, S. *Philos. Trans. R. Soc. London* **1956**, *248*, 449.
(28) White, L. R. *J. Colloid Interface. Sci.* **1983**, *95*, 286.
(29) Derjaguin, B. V. *Kolloid Z.* **1934**, *69*, 155.
(30) Bhattachrjee, S.; Ko, C.-H.; Elimelech, M. *Langmuir* **1998**, *14*, 3365.
(31) Hoek, E. M. V.; Bhattachrjee, S.; Elimelech, M. *Langmuir* **2003**, *19*, 4836.
(32) Shulepov, S. Y.; Frens, G. *J. Colloid Interface. Sci.* **1995**, *170*, 44.
(33) Shulepov, S. Y.; Frens, G. *J. Colloid Interface. Sci.* **1996**, *182*, 388.
(34) Czarnecki, J. *Adv. Colloid Interface Sci.* **1986**, *24*, 283.
(35) Sun, N.; Walz, J. Y. *J. Colloid Interface. Sci.* **2001**, *234*, 90.
(36) Lyklema, J.; Duval, J. To be submitted.
(37) Baker, N.; Holst, M.; Wang, F. *J. Comput. Chem.* **2000**, *21*, 1343.
(38) Elock, A. H.; McCammon. J. A. *Biophys. J.* **2001**, *80*, 613.
(39) Scheutjens, J. M. H. M.; Fleer, G. J. *J. Phys. Chem.* **1979**, *83*, 1619.
(40) Van Male, J. Ph.D. Thesis, Wageningen University, The Netherlands, 2003.

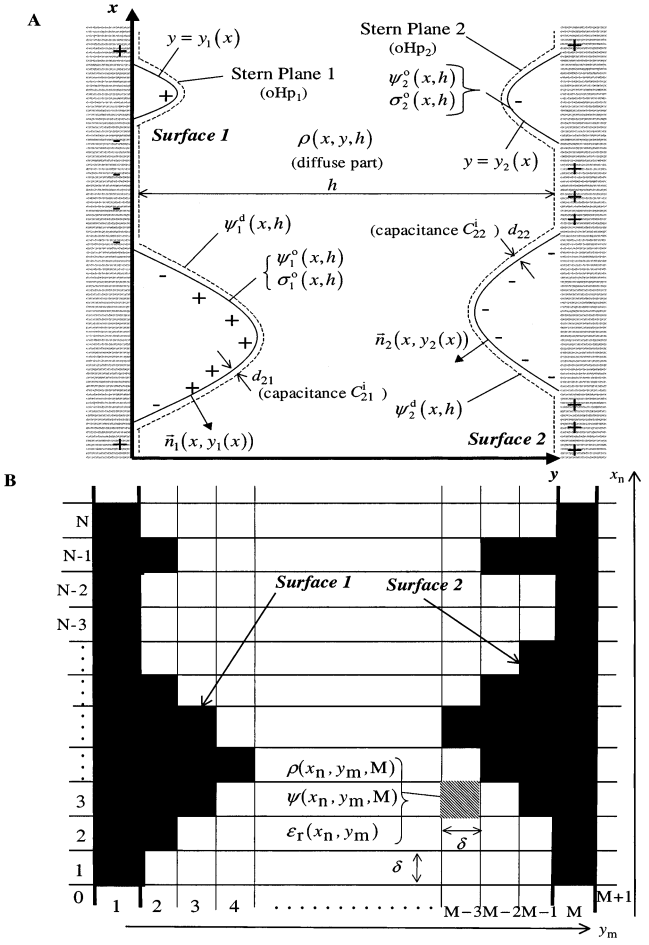

Figure 1. Heterointeraction between rough surfaces. (A) Continuous description (section 2.1) for the case where the regulation of the surface charges occurs across the diffuse part of the double layers and the outer Helmholtz layer. (B) Discrete representation (section 2.2) within a two-gradient mean-field lattice analysis. The inner and outer Helmholtz layers adjacent to the surface located at (x_n,y_m) may be modeled by specifying the dielectric permittivities of the cells (x_n,y_m) and $(x_n,y_m + 1)$, respectively.

2.1. Continuous Description: Potential and Charge Distributions, Gibbs Energy of Interaction. Two parallel, flat planes are separated by a distance h, as specified in Figure 1. The properties (either electrostatic or topological) of the left and right surfaces will be denoted with the subscript $j = 1$ and $j = 2$, respectively. The asperities placed on top of the flat surfaces define the roughness profiles, which can be described by the analytical expressions

$$y = y_1(x) \qquad y = h + \xi_2(x) = y_2(x) \tag{1}$$

for the coordinate system (x,y) as indicated in Figure 1. The surfaces are supposed to be uniform in the z-direction so that the problem can be described by the two spatial dimensions x and y only. The so-generated infinite ridges on surfaces 1 and 2 are parallel. At a given separation distance h, the electrostatic potential distribution $\psi(x,y,h)$ between the surfaces is described by the PB equation

$$\epsilon_0 \nabla\cdot[\epsilon_r(x,y)\vec{\nabla}\psi(x,y,h)] = -\rho(x,y,h) \tag{2}$$

where ϵ_0 is the dielectric permittivity of vacuum, $\epsilon_r(x,y)$ is the relative permittivity at the position (x,y), and $\rho(x,y,h)$ is the charge (per unit volume) at the position (x,y) and separation h. $\rho(x,y,h)$ is given by

$$\rho(x,y,h) = F\sum_i z_i c_i^{\infty} \exp[-z_i F\psi(x,y,h)/RT] \tag{3}$$

with R the gas constant, F the Faraday constant, and T the temperature. The index i refers to the ionic species i of valence z_i and bulk concentration c_i^{∞} (i.e., the concentration at infinite separation). The surface charge, denoted as $\sigma_j^{o}(x,h)$, at a separation distance h and position $(x,y_j(x))$, is related to the electric potential by the Gauss relation

$$\sigma_j^{o}(x,h) = -\epsilon_0\vec{\nabla}[\epsilon_r(x,y)\psi(x,y,h)]\cdot\vec{n}_j|_{y=y_j(x)} \tag{4}$$

where $\vec{n}_j$ is the unit normal vector to the surface j of which the components n_{xj} and n_{yj} are written

$$n_{xj} = -\lambda_j \frac{1}{\left(1 + \dfrac{dy_j(x)}{dx}\right)^{1/2}} \frac{dy_j(x)}{dx} \quad n_{yj} = \lambda_j \frac{1}{\left(1 + \dfrac{dy_j(x)}{dx}\right)^{1/2}} \tag{5}$$

with $\lambda_1 = +1$ and $\lambda_2 = -1$. We note that eq 4 tacitly implies that the electric field in the solid phase corresponding to surface j is zero. This might be a severe limitation for very rough surfaces and a particular type of materials such as semiconductors. However, computation of the field and potential further inside the solid phase can be easily implemented within the self-consistent field method adopted here providing detailed information on the charge distribution beyond the interface is available. For the sake of simplicity, we do not consider these refinements which necessarily call for introducing more parameters. There is a plethora of choices for expressing the boundary conditions required to solve eq 2. These may exclusively concern the surface potentials $\psi_j^{o}(x,h) = \psi(x,y_j(x),h)$ or the surface charges $\sigma_j^{o}(x,h)$. Mixed boundary conditions may be more realistic for certain types of heterointeractions. The surface potentials and/or charges may be taken constant with respect to h, uniform or actually depending on the position x. In that latter case, the assignment of a spatial surface distribution allows for the presence of chemical heterogeneities on top of surface roughness. In reality, there is no way of telling a priori if, upon interaction, the conditions of constant surface potential/surface charge are satisfied.

A more general analysis therefore calls for the inclusion of regulation mechanisms accounting for the adjustment of the potentials and/or charges upon double layer overlap. To that purpose, the occurrence of adsorption equilibria at the surfaces must be notified. In a previous analysis,[36] the issue of regulation of electric double layers at uniform charged colloids was revisited and generalized. To explicitly account for the ionic specificity, the double layers were described on the Gouy−Stern level. Provided that the characteristic length of the asperities introduced is larger than the distances from the surface d_{kj} ($k = 1$ refers to the inner Helmholtz layer and $k = 2$ to the outer Helmholtz layer, see Figure 1), the Stern layer is assumed to follow the contour of the roughness profile. Relaxing the condition of fixed surface charge, we consider surface charge regulation as it occurs between two interacting hydroxyl surfaces with adsorption sites denoted as ROH.

The charge-determining ions H^+ and OH^- can react at the surfaces following the equilibria

$$ROH \Leftrightarrow RO^- + H^+ \quad (6a)$$

$$K_{aj}(x) = \frac{[RO^-]}{[ROH]}\,\theta_{H^+}{}^{s}$$

$$ROH + H_2O \Leftrightarrow ROH_2{}^+ + OH^- \quad (6b)$$

$$K_{bj}(x) = \frac{[ROH_2{}^+]K_W}{[ROH]\theta_{H^+}{}^{s}}$$

where $\theta_{H^+}{}^{s}$ is the mole fraction of H^+ at the surfaces, K_W is the dissociation constant of water, and the brackets indicate surface concentrations given as moles of functional groups per unit surface area. To represent the situation of nonuniform charge distribution at the surfaces, we allow the reactions constants K_{aj} and K_{bj} to depend on the position x. Following the notation used in ref 36, all (local) K values (including K_W) written in eq 6 are dimensionless. $\sigma_j{}^{o}(x,h)$ is then related to the surface potential $\psi_j{}^{o}(x,h)$ by an adsorption isotherm of the type

$$\sigma_j{}^{o}(x,h) = 2FN_{sj}{}^{o}(x)\frac{\left(\frac{K_{aj}(x)K_{bj}(x)}{K_W}\right)^{1/2}\sinh\left\{\frac{F}{RT}[\psi_j{}^{N}(x) - \psi_j{}^{o}(x,h)]\right\}}{1 + 2\left(\frac{K_{aj}(x)K_{bj}(x)}{K_W}\right)^{1/2}\cosh\left\{\frac{F}{RT}[\psi_j{}^{N}(x) - \psi_j{}^{o}(x,h)]\right\}} \quad (7)$$

$N_{sj}{}^{o}(x)$ values are the local densities of adsorption sites per unit area for surface j and the potentials $\psi_j{}^{N}(x)$ are defined by

$$\psi_j{}^{N}(x) = -2.303(pH - pH_j{}^{o}(x)) \quad (8)$$

with the local point of zero charge $pH_j{}^{o}(x)$ for surface j given by

$$pH_j{}^{o}(x) = \frac{1}{2}(pK_{aj}(x) + pK_W - pK_{bj}(x)) \quad (9)$$

In the case of specific adsorption of ions onto the surfaces, the resulting local adsorbed charges, denoted as $\sigma_j{}^{i}(x,h)$, are assumed to be related to the potentials $\psi_j{}^{i}$ at the iHp by the Frumkin−Fowler−Guggenheim (FFG) equation in the form

$$\sigma_j{}^{i}(x,h) = \frac{z_i e N_{sj}{}^{i}(x)\theta_i K_{ij}\exp\left(-\frac{z_i F}{RT}\psi_j{}^{i}(x,h)\right)}{1 + \theta_i K_{ij}\exp\left(-\frac{z_i F}{RT}\psi_j{}^{i}(x,h)\right)} \quad (10)$$

We consider only one type of ion (valence z_i) at the iHp of which the mole fraction in the solution is θ_i. $N_{sj}{}^{i}(x)$ is the local number of adsorption sites per unit area for ion i on surface j, and

$$K_{ij} = \exp(-\Delta_{ads}G_{m,ij}/RT) \quad (11)$$

where $\Delta_{ads}G_{m,ij}$ is the molar Gibbs energy of specific adsorption for ion i at surface j. We consider that for the different patches along the surfaces, $\Delta_{ads}G_{m,ij}$ is the same and thus is independent of x. The local electrostatic contributions to the ionic adsorption are included in the exponential function. The charge density $\rho(x,y,h)$ in the diffuse part follows directly from the potential distribution, as expressed by Gauss' law. The pair of interfaces as a whole is electroneutral so that for every h we have the relation

$$\int\int_{xy}\rho(x,y,h)\,dx\,dy + \sum_j\{\int_{surface_j}\sigma_j{}^{o}(x,y_j(x),h)\,dx + \int_{iHp_j}\sigma_j{}^{i}(x,y_j(x) + d_{1j},h)\,dx\} = 0 \quad (12)$$

where we have eliminated the distance of normalization in the z-direction. The set of nonlinear eqs 1−12 must be solved consistently so as to derive the anisotropic potential and charge distributions. Once that is done, the electrostatic interaction energy can be evaluated from the charging energy for both surfaces. These are functions of h and position x. We shall denote them as $\Delta G_j(x,h)$, where the symbol Δ refers to the difference with respect to the reference state, i.e., the uncharged surface. $\Delta G_j(x,h)$, counted per unit area, contains a chemical contribution, as resulting from the surface charge regulation and/or the specific adsorption of ions at the iHp and an electrostatic contribution. Rewriting the result for isolated double layers,[41] we have

$$\Delta G_j(x,h) = -\frac{(\sigma_j{}^{o}(x,h))^2}{2C_{1j}{}^{i}} - \frac{(\sigma_j{}^{i}(x,h))^2}{2C_{2j}{}^{i}} - \int_\infty^h\frac{\partial(\sigma_j{}^{d}(x,h)\psi_j{}^{d}(x,h))}{\partial h}\,dh \quad (13)$$

where the diffuse charges $\sigma_j{}^{d}$ are given by Gauss' law

$$\sigma_j{}^{d}(x,h) = -\epsilon_0\vec{\nabla}[\epsilon_r(x,y)\psi(x,y,h)]\cdot\vec{n}_j|_{y=y_j(x)+d_{2j}} \quad (14)$$

$C_{kj}{}^{i}$ values are the capacitances of the inner and outer Helmholtz layers as defined by the corresponding d_{kj} and the relative dielectric permittivities $\epsilon_r(x,y)$ taken constant in these layers. $\psi_j{}^{d}(x,h)$ in eq 13 refers to the potential at the oHp. The total electrostatic interaction energy G is then obtained by integration of eq 13 over the exact surface geometries after subtracting the charging energy of the isolated electric double layers (i.e., at $h \to \infty$)

$$G(h) = \sum_j\frac{1}{A_j}\left\{\int\int_{y=y_j(x)}[\Delta G_j(x,h) - \Delta G_j(x,h\to\infty)]\,dx\,dy\right\} \quad (15)$$

with A_j the total area of surface j. At this point of the analysis, it is useful to emphasize that the use of the DA[28,29] and the SEI technique[30,31] for estimating G is mainly motivated by the existence of analytical expressions for the interaction Gibbs energy at constant surface potential or constant surface charge between flat parallel planes. However, in the more general situation of interaction between regulating one-dimensional double layers, no (general) analytical equation has been formulated so far. Therefore, to account for these cases, DA and SEI methods, putting aside the limitations they necessarily imply, should be combined with numerical integration of eqs 1−12 in the flat geometry. More specifically, as far as SEI is concerned, the authors emphasize its suitability for the constant potential case but are more elusive about its feasibility for the other interaction situations.[42] In that

(41) Lyklema, J. In *Fundamentals of Interface and Colloid Science*; Academic Press: San Diego, CA, 1995; Vol II, Chapter 3.

respect, the self-consistent-field theory we use allows a higher degree of flexibility since it enables solving eqs 1−15 for any geometries and regulating boundary conditions as expressed by eq 1 and eqs 7 and 10, respectively.

2.2. Self-Consistent-Field Lattice Theory. Electrostatics. In this section, we describe the problem previously sketched as it is tackled within a self-consistent-field scheme based on the theory of Scheutjens and Fleer.[39] In the numerical evaluation of the theory, the space between the two surfaces is confined in a two-dimensional lattice of size $N \times M$. N and M represent the number of plane-parallel thin layers of thickness δ (0.3 nm) in the x and y directions, respectively (Figure 1). The charges and potentials are smeared-out in the z-direction. We describe here the situation of a flat lattice, but cylindrical or spherical geometries are also possible.[40] The layers are filled with solvent molecules and (hydrated) ions of which the spatial distribution is governed by the Boltzmann statistics. The volume fraction of ion i at the position (x,y) is denoted as $\varphi_i(x,y)$. All sites have equal volume δ^3. Unlike the PB theory which considers point charges, the ions are given here a finite size. It is done by describing the local potential as the sum of the potential as defined within the PB theory and a potential, which can be seen as the isothermal work which must be performed (in the incompressible limit) to carry a unit with volume δ^3 from a position infinite to a position corresponding to a cell (x,y). As long as $\kappa\delta < 1$ (with κ^{-1} the Debye length), the potential and charge distributions as derived from the PB equation including finite volume for the ions are the same as those obtained within the point charge approximation. For $\kappa\delta > 1$ (high electrolyte concentration), classical Poisson−Boltzmann theory fails to describe the electrostatics since the steep potential drop close to the surface (strong electric field or equivalently high surface charge) takes place within distances comparable with ion dimensions. In this latter situation, it is necessary to introduce a Stern layer adjacent to the surface and of which the thickness equals one or two times the ion radius. Discretization on the δ-length scale as in the current self-consistent field analysis automatically includes such a Stern layer correction. Each site interacts with all neighboring sites through chemical and electric forces. The mean field principle enters in that an ion interacts with the local average of all other ions, instead of interacting with other ions taken individually. The discretization of the PB equation is done using a capacitor model.[43] Within this model, the charges are assumed to be located on the planes in the center thus forming a multiplate capacitor of the same geometry as the lattice. The space can therefore be viewed as the succession of M Stern layers, with relative dielectric permittivities $\epsilon_r(x,y)$ being assigned at will. We stress that δ not only is a numerical parameter (required for the discretisation of the electrostatics) but also has a physical origin, connected to the nature of the Stern layer itself (excluded volume for the ions taken into account). The positions are readily obtained from the relations

$$n \in [0,\mathrm{N}]: \qquad x_n = n\delta + \frac{1}{2} \tag{16}$$

$$m \in [0,\mathrm{M}]: \qquad y_m = m\delta + \frac{1}{2} \tag{17}$$

The discretized form taken by the PB equation is

$$\begin{aligned}\bar{\epsilon}_r(x_n,y_m)\psi(x_n,y_m) = 2\frac{\rho(x_n,y_m)}{\epsilon_0} + \\ [\epsilon_r(x_n,y_m+1) + \epsilon_r(x_n,y_m)]\psi(x_n,y_m+1) + \\ [\epsilon_r(x_n,y_m) + \epsilon_r(x_n,y_m-1)]\psi(x_n,y_m-1) + \\ [\epsilon_r(x_n+1,y_m) + \epsilon_r(x_n,y_m)]\psi(x_n+1,y_m) + \\ [\epsilon_r(x_n,y_m) + \epsilon_r(x_n-1,y_m)]\psi(x_n-1,y_m)\end{aligned} \tag{18}$$

with the quantity $\bar{\epsilon}_r(x_n,y_m)$ defined by

$$\begin{aligned}\bar{\epsilon}_r(x_n,y_m) = \epsilon_r(x_n,y_m+1) + \epsilon_r(x_n,y_m-1) + \\ \epsilon_r(x_n+1,y_m) + \epsilon_r(x_n-1,y_m) + 4\epsilon_r(x_n,y_m)\end{aligned} \tag{19}$$

The local charge density $\rho(x_n,y_m)$ is related to the ion volume fractions by

$$\rho(x_n,y_m) = \frac{1}{\delta^3}\sum_i ez_i\varphi_i(x_n,y_m) \tag{20}$$

and the electrostatic interaction energy (in k_BT per unit area) by

$$G_{el} = \frac{F}{2k_BT\delta^2}\sum_n\sum_m \psi(x_n,y_m)\sum_i z_i\varphi_i(x_n,y_m) \tag{21}$$

where k_B is the Boltzmann constant.

Reaction Equilibria at the Surfaces and/or at the iHp's. A possibility offered by the sfbox program is the implementation of reaction equilibria at the surfaces, e.g., the specification of protonation and complexation reactions. For a given position x_n along the surface j, we can write such reactions in a concise form as follows

$$\sum_q \upsilon_q^{x_n,j} S_q^{x_n,j} = 0 \tag{22}$$

where S refers to both reactants and products. The index q denotes the species q involved in the reaction and the $\upsilon_q^{x_n,j}$ values are the stoichiometric coefficients. We follow the convention $\upsilon_q^{x_n,j} > 0$ for q product and conversely for the reactant. The associated thermodynamic constant $K_j(x_n)$ is related to the bulk volume fractions φ_q^∞ of the species q by

$$\ln(K_j(x_n)) = \sum_q \upsilon_q^{x_n,j}\ln(\gamma_q\varphi_q^\infty) \tag{23}$$

with γ_q the activity coefficient of q. At constant temperature, the local adsorption Gibbs energy at surface j, denoted as $G_j(x_n)_{chem}$ (in k_BT per unit area), and corresponding to equilibrium 22 is given by

$$G_j(x_n)_{chem} = -\frac{1}{k_BT}\sum_q \Gamma_q^j(x_n)\mu_q \tag{24}$$

where $\Gamma_q^j(x_n)$ is the amount (moles) per unit area of adsorbed species q at the position x_n on surface j and μ_q the chemical potential of q given by

$$\mu_q = k_BT\ln(\gamma_q\varphi_q^\infty) \tag{25}$$

Equation 24 can be rearranged using the relation valid at thermodynamic equilibrium

(42) Bhattachrjee, S.; Elimelech, M. *J. Colloid Interface. Sci.* **1997**, *193*, 273.

(43) Barneveld, P. A.; Hesselink, D. E.; Leermakers, F. A. M.; Lyklema, J.; Scheutjens, J. M. H. M. *Langmuir* **1994**, *10*, 1084.

$$\sum_q \upsilon_q^{x_n,j}\mu_q = 0 \tag{26}$$

and the mass balance relation (the total number of adsorption sites is constant). $\Gamma_q^j(x_n)$ is related to the local charge density by

$$\sigma_j^{o,i}(x_n) = F\sum_q z_q\Gamma_q^j(x_n) \tag{27}$$

where the superscript o holds for (protonation) reactions taking place at the surface and the superscript i for (complexation) reactions at the iHp. We note in passing that the adsorption isotherms as written in eqs 7 and 10 may be obtained by writing the condition stating that, at equilibrium, the electrochemical potential of the free ions in the bulk solution is equal to that of the corresponding ions bound at the surface.

Using the appropriate boundary conditions (constant charge, constant potential, or boundary regulation conditions) for different separation distance h, i.e., different M, the potential distribution $\psi(x_n,y_m)$, the charge density $\rho(x_n,y_m)$, and volume fraction $\varphi_{i,q}(x_n,y_m)$ are computed in an iterative scheme where the potential is taken as variable and updated until a self-consistent solution is obtained. Electrostatic mirrors placed at the layers 0 and $M + 1$ ensure the condition of zero-electric field at these coordinates and the condition of electroneutrality for the pair of colloids; i.e., the relation $\sum_n\sum_m\rho(x_n,y_m) = 0$. Then the total interaction energy G at a given M is yielded by

$$G(M) = G_{el}(M) + \sum_j\sum_n G_j(x_n,M)_{chem} \tag{28}$$

which is the pendant of eq 15.

Generation of the Surface Roughness. The surface profile is assigned following what we call a Lego type procedure. More specifically, the positions (n,m) along the surface to be modeled are "frozen", meaning that the corresponding sites will effectively act as solid substrate. These sites are inaccessible for molecules (ions, water). The chemical and electrostatics characteristics of these (pK values, adsorption energies, number of sites, surface charges, and ϵ_r values) may differ from the ones chosen for the flat surface on top of which the asperities are grafted. An example is given in Figure 1. The asperities may be of the type "protusion" or "depression", i.e., convex or concave, respectively. One or both surfaces may contain asperities.

3. Results and Discussion

The sfbox program was first tested for a number of 1D-interaction situations where analytical expressions, generally given in the Debye−Hückel (DH) approximation,[36] are available. Good agreement was found in the three geometries (flat, cylindrical, spherical) for the separation range effectively corresponding to the DH regime (not shown). Results including charge/potential regulations in the conditions of constant surface potential/charge were also successfully compared to those expected on the basis of the expressions given by Hogg et al.[44] and Usui.[45] Considering the multiparameter nature of the issue presented in the previous section, the variety of situations that can be envisaged is virtually infinite. We shall here focus on a few characteristic examples, which clearly highlight the paramount importance of roughness and chemical nonuniformities in determining electrostatic interaction energy.

As a starting point, we analyze the interaction between a flat plate ($j = 2$) and a flat surface ($j = 1$) on which a bar of height h_a and width δ is positioned. Figure 2 shows the results for different h_a and different bulk volume fractions φ_b^∞ of a 1:1 electrolyte. The surface charges are kept constant upon interaction, and the charge density carried by the asperity, denoted as σ_{a1}^o, is the same as the one carried by its supporting plane, denoted as σ_{s1}^o. In the following, all the charge densities σ of interest will be given in elementary charge per unit cell (0.01 elementary charge per unit cell = 1.78 μC cm^{-2}). Variation in φ_b^∞ allows for tuning the range of electrostatic double layer (EDL) interaction expressed in terms of the Debye length κ^{-1}. In the framework of the Debye−Hückel regime, κ^{-1} is read from the slope of the plot log(G) versus h. For $\kappa h_a \ll 1$ (low φ_b^∞), the roughness of the left surface is "unseen" or, otherwise stated, screened by the range of EDL interactions. The resulting interaction curve is essentially the same as that between two flat surfaces. For $\kappa h_a \approx 1$ or $\kappa h_a > 1$ (high φ_b^∞), the spatial detail of the surface profile, that is, the characteristic size of the asperity, becomes comparable to or even overrules the range of EDL interaction. Upon increasing φ_b^∞, this is materialized by a splitting of the interaction curves calculated for different h_a. At given φ_b^∞, the larger the h_a, the stronger the repulsion (the surface charges σ_j^o have the same sign). At given h_a, the larger the φ_b^∞, the less the repulsion because of the screening effect of the counterions. The numerical results may be compared with those expected on the basis of the scaling technique proposed by Derjaguin (Derjaguin approximation, DA). We mention however that this latter is not expected to fit the results since the surface geometry considered here is not "smooth". The comparison is only relevant in the sense that it clearly highlights the origin of the discrepancies between the numerical and DA approaches. For the simple geometry of surface roughness chosen, we have

$$G_{DA}(h_a,M) = \frac{N-1}{N}G^{(flat)}(M) + \frac{1}{N}G^{(flat)}(M - h_a/\delta) \tag{29}$$

where the superscript (flat) is read as "the interaction energy between flat parallel plates (without any asperity)". For high κh corresponding to weak overlap of the EDL, the DA well predicts the computed G but underestimates G for low κh and high κh_a (Figure 2). In these regimes, the interactions between elements of the surfaces that do not face each other contribute for an overall repulsion that is not taken into account by the DA scaling technique. Similar results are obtained when increasing the width of the asperity at given κh_a.

In the next case, the charge density carried by the asperity differs in size and sign from that (positive) at the surface where it is grafted (Figure 3). Besides, we choose $\sigma_2^o > 0$. As intuitively expected, when increasing κh_a, the interaction then progressively changes from repulsion to attraction. For high κh_a, the sign and magnitude of the interaction are predominantly determined by the chemical properties of the asperity and of course by those of the opposed surface $j = 2$.

In Figure 4, two protrusions of the same height h_a are placed on the left surface ($j = 1$). For the sake of convenience, we shall denote the surface charge densities of the asperities as $\sigma_{a1,2}^o$. We have arbitrarily chosen $\sigma_{a1,2}^o = 2\sigma_{s1}^o$. The respective positions of the two asperities

(44) Hogg, R.; Healy, T. W.; Fuersteneau, D. W. *Trans. Faraday Soc.* **1966**, *62*, 1638.
(45) Usui, S. *J. Colloid Interface Sci.* **1973**, *44*, 107.

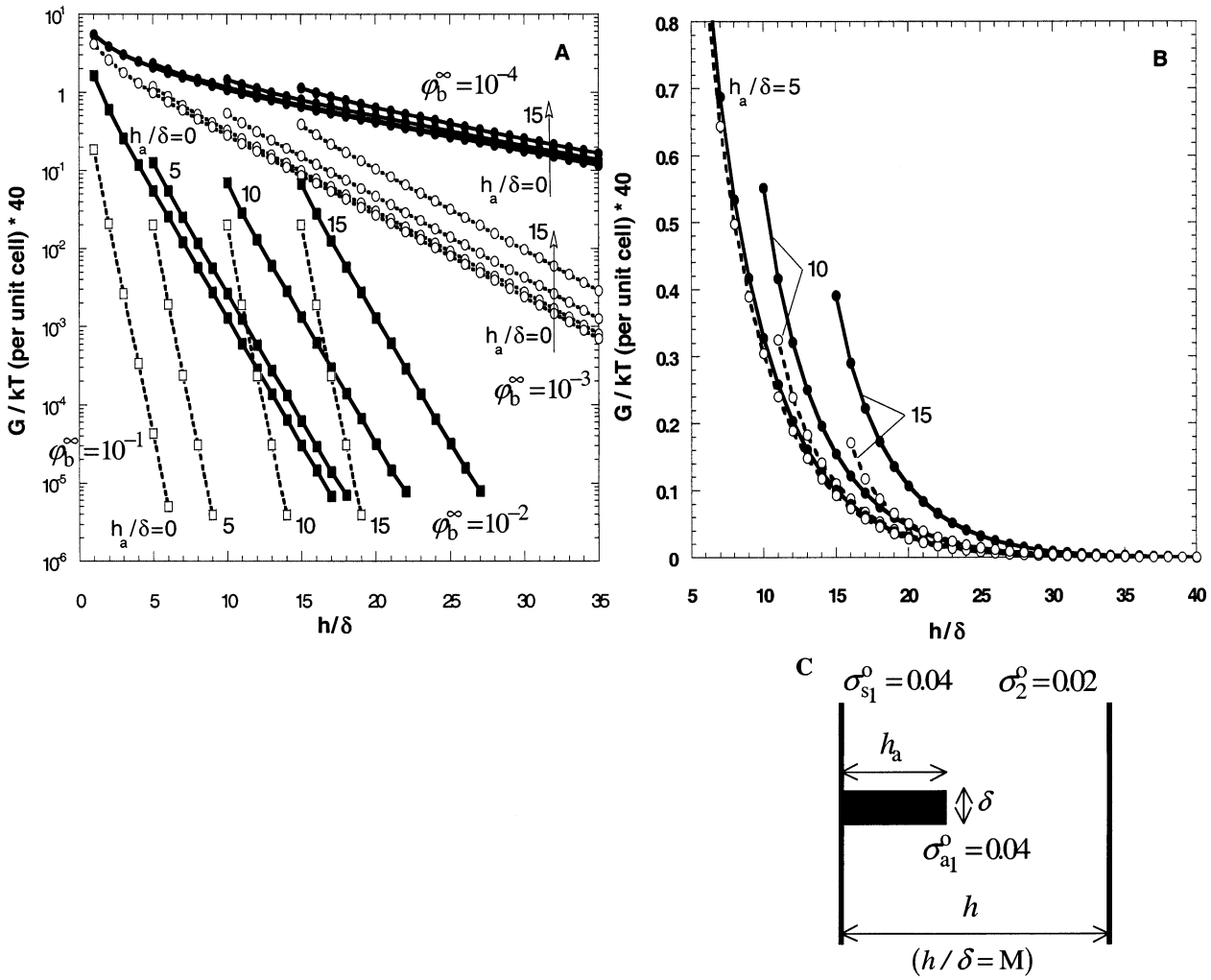

Figure 2. (A) Interaction Gibbs energy corresponding to the situation depicted in the scheme panel C. In panel B, the numerical results (full lines) are compared to the predictions based on the DA approximation (dashed lines) for $\varphi_b^\infty = 10^{-3}$ ($\kappa^{-1}/\delta \approx 4.3$). No Stern layers are explicitly considered (ϵ(Stern) = ϵ(diffuse part) = 78).

are changed by varying their separation distance l in the x-direction. To highlight the eventual effects of l on G, h_a was chosen such that $\kappa h_a > 1$. For the simplistic configuration chosen, the dependence of G on l is not very pronounced but still the results are illustrative of the electrostatic anisotropy developed in the x-direction. To qualitatively understand the results, one may reason in terms of the quantity κl. We emphasize however that the scaling distance κ^{-1} along the x-direction is arbitrary since this latter primarily indicates the extent of the EDL in the y-direction. The physically relevant Debye length, κ^{*-1}, is actually a function of x. For the sake of illustration, we present in the Appendix a way to derive the functionality $\kappa^{*-1}(x)$ in the cases where $h_a/l < 1$. Getting back to Figure 4 and keeping in mind the previous point, it is clear that l does not affect G for large κh, as intuitively expected. At lower κh, provided that the double layers between the two asperities (in the x-direction) do not overlap ($\kappa l \gg 1$), G remains independent of l (high φ_b^∞). In the other case, weak overlap of the EDL along the rough surface ($\kappa l > > 1$) leads to a slight additional repulsion in the overall interaction curve and strong overlap ($\kappa l \ll 1$) to an attractive contribution. In this latter situation, the local electrostatic repulsion between the asperities is completely screened and therefore not reflected in G. If the absolute magnitude of the charge on the two asperities is increased, these effects are magnified. The DA approximation cannot predict any dependence of G on l since the corresponding scaling of the interaction energy between flat plates is done according to the y-direction only.

In Figure 5, we analyze the situation where $\sigma_{a1}{}^o = -\sigma_{a2}{}^o (>0)$ and $\kappa l \gg 1$ (same h_a for the two asperities and $\kappa h_a > 1$). The total charge carried by the rough surface is kept constant (in the example given, $\sigma_{a1}{}^o + \sigma_{a2}{}^o + \sigma_{s1}{}^o = 0$). The results are given for different $\sigma_{a1}{}^o$ and $\varphi_b^\infty = 5 \times 10^{-3}$. Contrary to first intuition, the overall interaction actually depends on $\sigma_{a1}{}^o$, the interaction becoming repulsive upon increase of $\sigma_{a1}{}^o$. The results can be qualitatively understood by means of the DA approximation, which is now written

$$G_{DA}(\sigma_{a1,2}{}^o, M) = \frac{N-2}{N} G^{(flat)}(M) + \frac{1}{N} G^{(flat)}(\sigma_{a1}{}^o, M - h_a/\delta) + \frac{1}{N} G^{(flat)}(\sigma_{a2}{}^o, M - h_a/\delta) \quad (30)$$

where the two last terms in the right-hand side of eq 30 stand for the energy of interaction between a flat plate carrying the charge $\sigma_{a1}{}^o$ (or $\sigma_{a2}{}^o$) and a flat plate carrying the charge $\sigma_2{}^o$. The sign and magnitude of the overall interaction result from the asymmetry of the interactions between the asperities taken separately and the surface $j = 2$. For the example given, the DA approximation

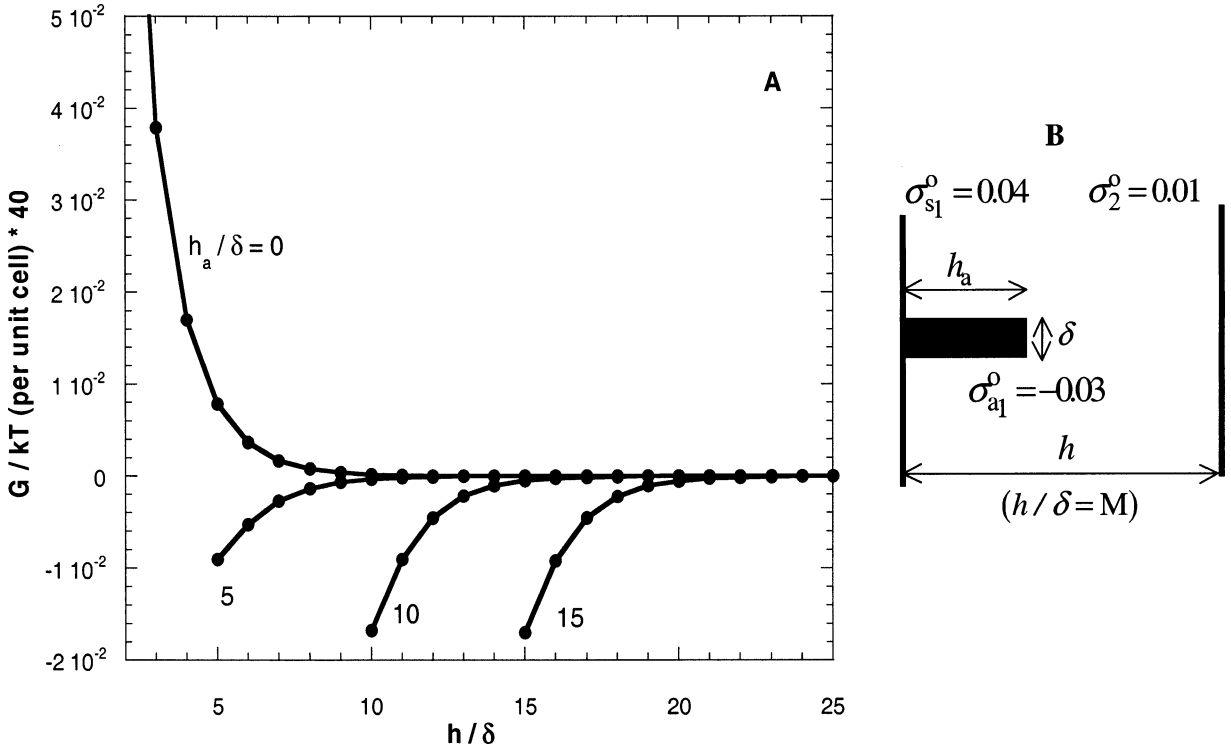

Figure 3. (A) Interaction Gibbs energy corresponding to the situation depicted in the scheme panel (B) for $\varphi_b^\infty = 10^{-2}$. No Stern layers are explicitly considered (ϵ(Stern) = ϵ(diffuse part) = 78).

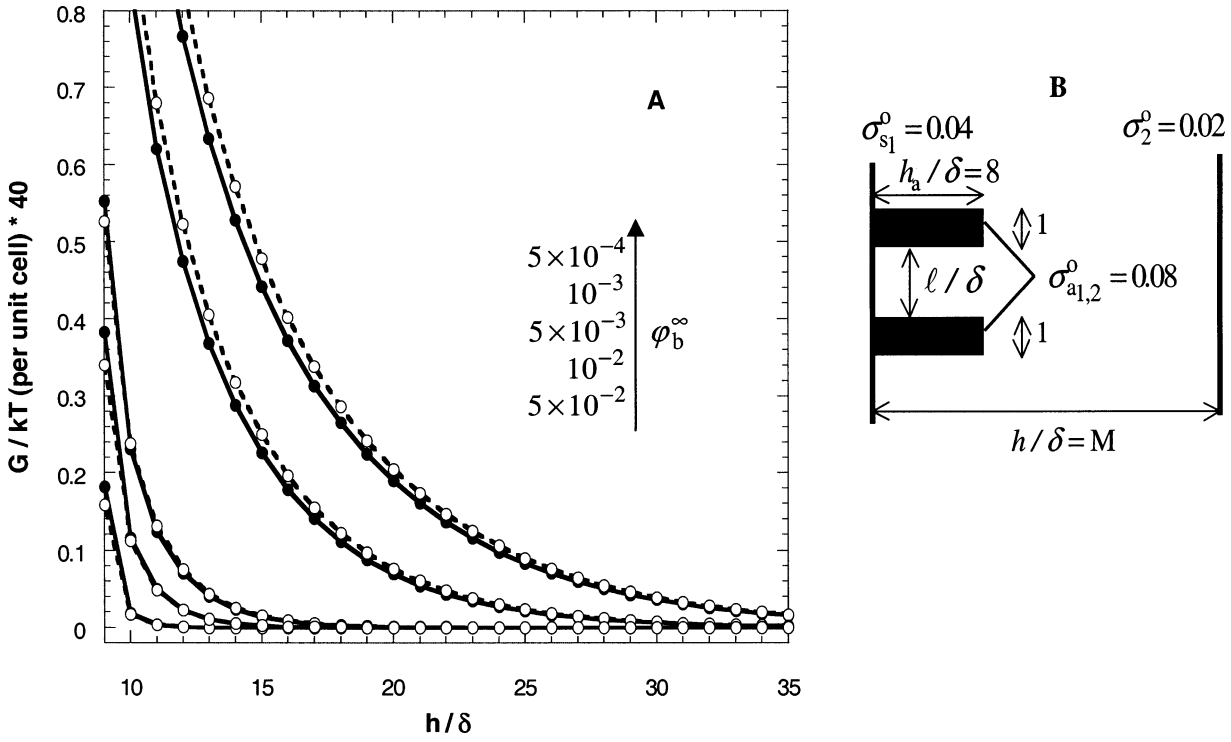

Figure 4. (A) Interaction Gibbs energy corresponding to the situation depicted in the scheme panel B. The full and dashed lines stand for $l/\delta = 1$ and $l/\delta = 30$, respectively. The bulk volume fraction of 1:1 electrolyte is indicated. In this picture, the dielectric permittivity ϵ_r in the outer Helmholtz layers is set to 20, otherwise 78.

qualitatively yields the same results as those obtained by the numerical analysis and quantitatively we have $G_{DA} > G$. For $\sigma_2^o = 0$, changing in the charge $\sigma_{a1}^o = -\sigma_{a2}^o$ carried by the protrusions would affect the local distribution of the countercharge but not the total Gibbs energy of interaction.

In Figure 6, specific interaction of anions with both surfaces is taken into account. The characteristics of the inner and outer Helmholtz layers as well as the molar Gibbs energies of adsorption are specified. Upon increase of the asperity size, the interaction gradually changes from repulsion to attraction. The total adsorbed charge at the iHp_1 which comes into play for the determination of G is given by the summation of the local adsorbed charges along the contour of surface 1. For low κh_a, this charge does not suffice to reverse the sign of the total charge

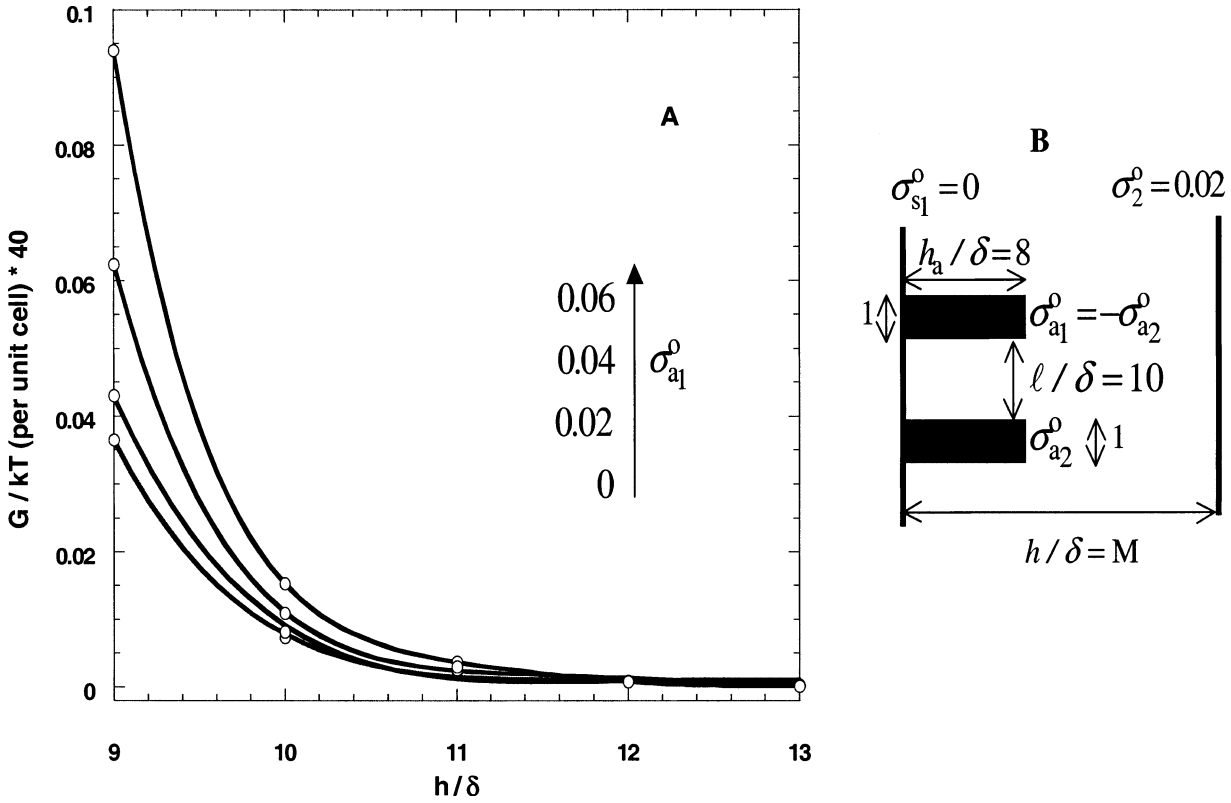

Figure 5. (A) Interaction Gibbs energy corresponding to the situation depicted in the scheme panel B. The charges carried by the asperities are indicated. In this picture, the dielectric permittivity ϵ_r in the outer Helmholtz layers is set to 20 (otherwise 78). $\varphi_b^\infty = 5 \times 10^{-3}$.

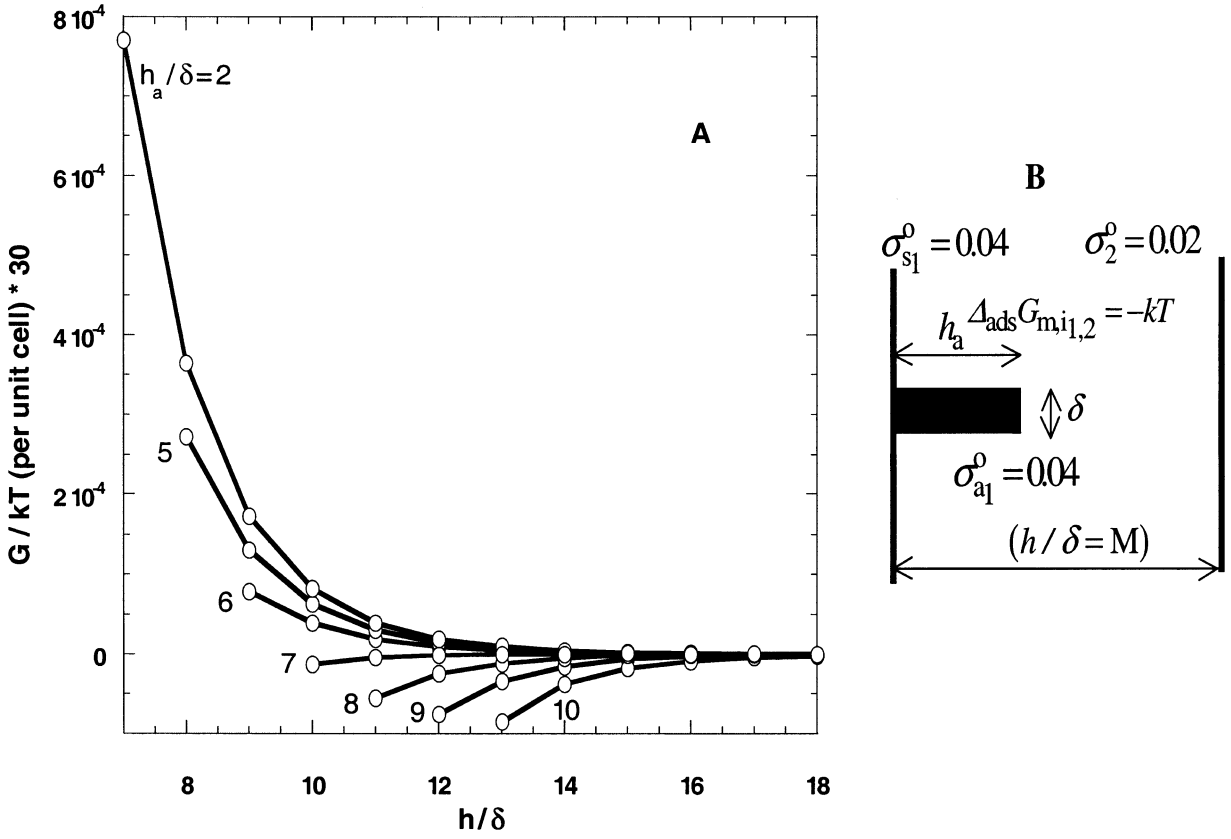

Figure 6. (A) Interaction Gibbs energy corresponding to the situation depicted in the scheme panel B. $\varphi_b^\infty = 10^{-2}$. For both surfaces, the dielectric permittivities ϵ_r in the inner and outer Helmholtz layers are set to 20 and 50, respectively. In the diffuse part, $\epsilon_r = 78$. Specific adsorption of anions on both surfaces is considered.

carried by surface 1, so that repulsion ensues ($\sigma_2^o > 0$). When κh_a is increased, the electric and chemical properties of the asperity prevail in the determination of G (see Figure 2) so that, roughly speaking, the only charge distribution

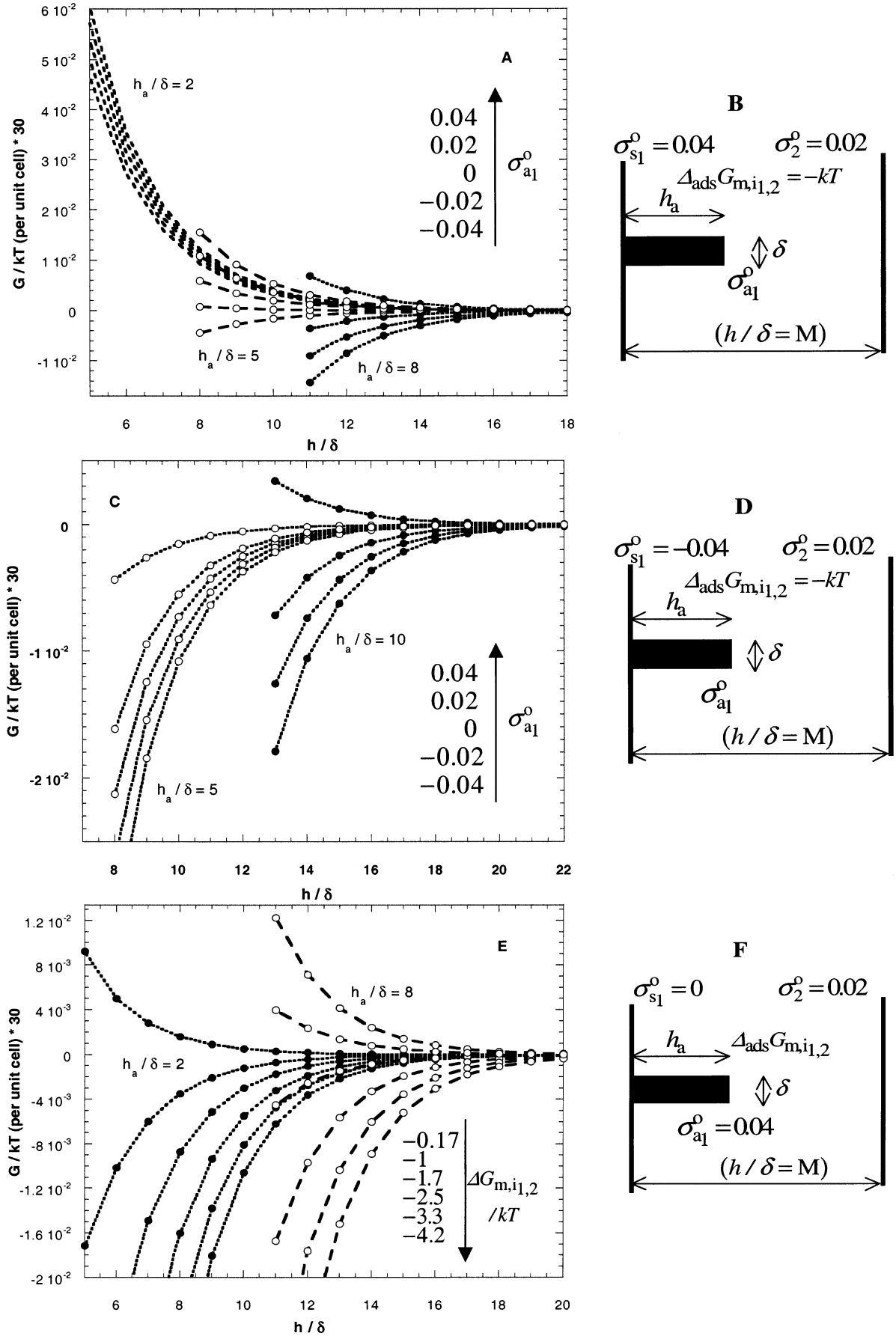

Figure 7. Interaction Gibbs energy computed for different topological/chemical heterogeneities (indicated) located at surface 1. The schemes in panels B, D, and F refer to the set of curves of panels A, C, and E, respectively. $\varphi_b^\infty = 5 \times 10^{-3}$. For both surfaces, the dielectric permittivities ϵ_r in the inner and outer Helmholtz layers are set to 20 and 50, respectively. In the diffuse part, $\epsilon_r = 78$. Specific adsorption of anions on both surfaces is considered.

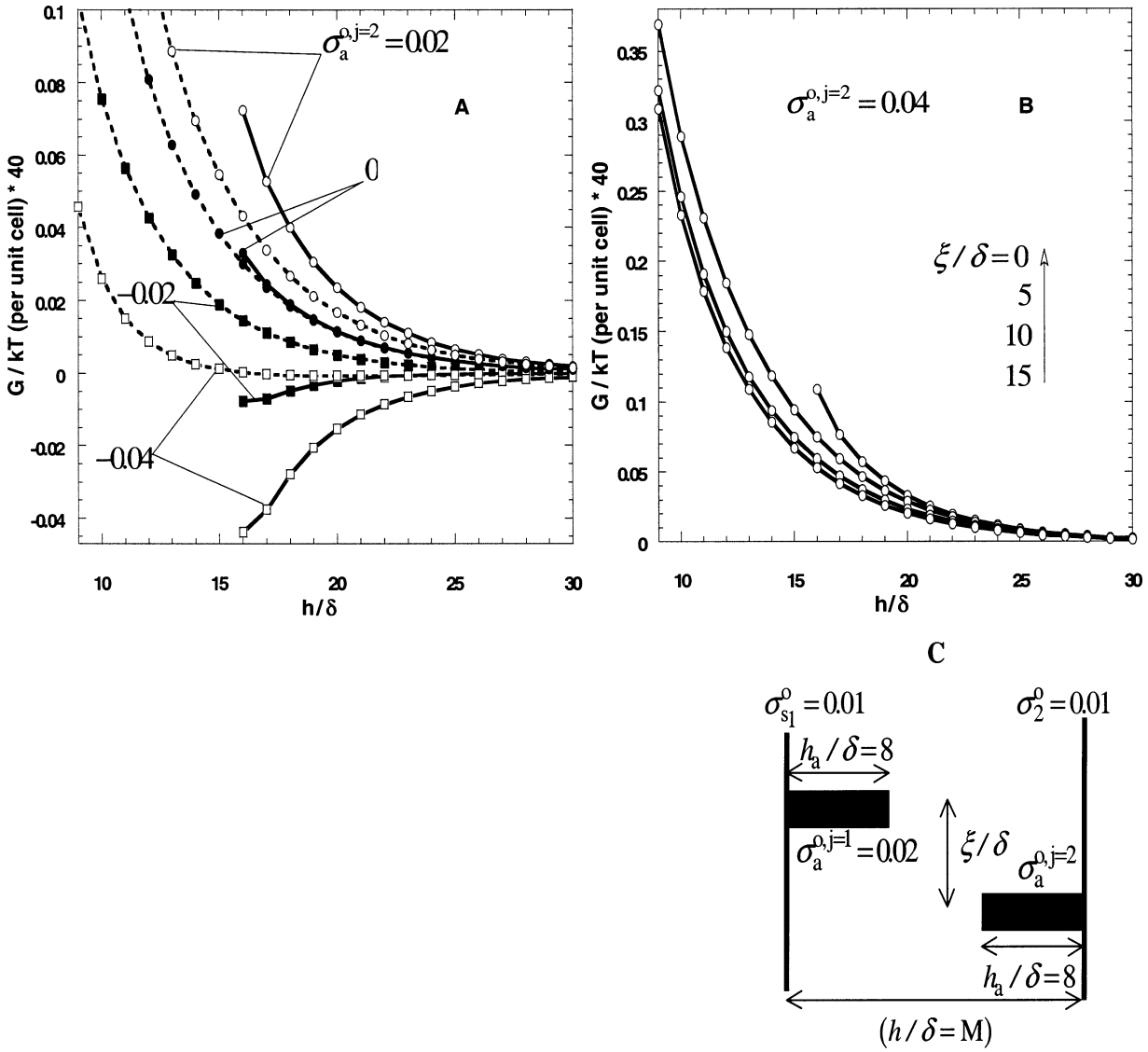

Figure 8. Interaction Gibbs energy (A and B) corresponding to the situation depicted in scheme C. In panel A, the dashed and full lines stand for $\xi/\delta = 15$ and $\xi/\delta = 0$, respectively. Overall $\varphi_b^{\infty} = 10^{-3}$. The dielectric permittivity ϵ_r in the outer Helmholtz layers is set to 20 (otherwise 78).

in the vicinity of the asperity, or otherwise stated, the local regulation features at the asperity become of importance. The total effective (apparent) charge carried by surface 1 decreases and now superequivalent adsorption occurs, thus leading to attraction.

In Figure 7, interaction curves are given for different combinations of $\sigma_{a1}{}^{o}$, $\sigma_{s1}{}^{o}$, $\Delta_{ads}G_{m,i1,2}$, and various values of κh_a. The results, qualitatively in line with intuition, again illustrate the possibility of sign reversal of the overall interaction as the result of the presence of morphological/chemical heterogeneities.

Next, we analyze the situation where both surfaces contain an asperity, the sizes of these being identical. The charge carried by the asperity positioned at surface $j = 2$, denoted as $\sigma_a{}^{o,j=2}$, is varied in magnitude as well as in sign compared to that of the asperity at surface $j = 1$ ($\sigma_a{}^{o,j=1}$ chosen positive). The spatial shift between the protrusions is denoted as ξ. For high h, G is independent of ξ for reasons already mentioned. At lower h, for $\sigma_a{}^{o,j=1}\sigma_a{}^{o,j=2} > 0$, the results presented in Figure 8 indicate that for a given separation distance, the energy of interaction increases when decreasing ξ and increasing $\sigma_a{}^{o,j=2}$. The repulsive energy is maximum when the two protrusions are in line ($\xi = 0$). For $\sigma_a{}^{o,j=1}\sigma_a{}^{o,j=2} < 0$, decrease of ξ alters G both in amplitude and in sign because of the increasing contribution of the attractive bar−bar interaction. Upon increase of ξ, the interaction energy tends to a constant value as the result of the diminishing of the extension of the double layers overlap in the direction given by the extremities of the two asperities. The conclusions pertaining to the effect of ξ on G are in line with those derived by Tsao[46] for electrostatic interactions between two corrugated surfaces. In this paper, the interaction energy is computed using a perturbation theory valid for smooth corrugation and only the case of uniformly charged surfaces is examined.

As a final example, we compute the interaction energy between two plates of which the surface charges are determined by the charge-determining ions H^+ present in the solution (equilibria 6a,b). Surface ($j = 2$) is flat and surface ($j = 1$) contains a protusion of height h_a. Figure 9 shows the results for different h_a and different pH values. By choice of the pK values, we have $pH_{j=1}{}^{o} = 4.5$ and $pH_{j=2}{}^{o} = 8.5$. The results for $h_a = 0$ have already been discussed in detail in ref 36. Upon increase of h_a, the repulsion (pH = 3, 10) or the attraction (pH = 6, $pH_{j=1}{}^{o}$)

(46) Tsao, H.-K. *J. Colloid Interface. Sci.* **1999**, *216*, 370.

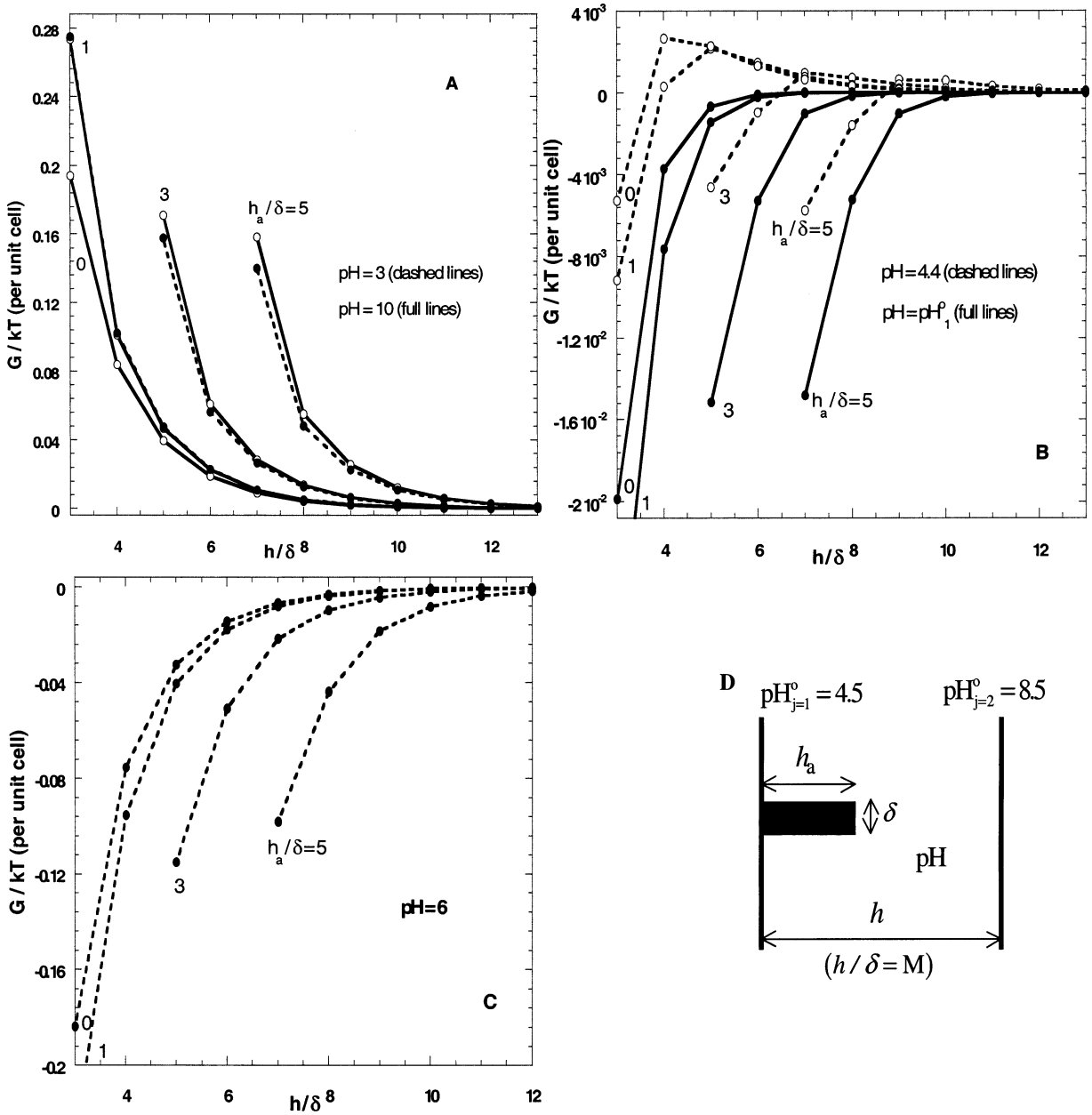

Figure 9. Interaction Gibbs energy (A−C) corresponding to the situation depicted in the scheme panel D. The results are shown for different pH values and h_a, as indicated. $\varphi_b^\infty = 10^{-2}$. The dielectric permittivity ϵ_r in the outer Helmholtz layers is set to 40 (otherwise 78).

increases at given h. For the case where induction takes place (pH = 4.4), the transition long-range repulsion/short-range attraction occurs at longer separation distance. The 2D morphology as introduced for the left surface generates a loss of the symmetry of G with respect to the pH, denoted pH_1 and pH_2, and verifying $pH_1 - pH_{j=1}^{o} = pH_{j=2}^{o} - pH_2$ (see panel A). The trends constitute the pendant of the results discussed in Figure 2 for the constant surface charge situation.

4. Conclusions

The electrostatic contribution to the Gibbs energy of interaction between heterogeneous surfaces has been evaluated for simple geometrical models and various boundary conditions. These are pertaining to the surface charges carried by the asperities and by the planar surfaces on which they are grafted. The analysis presented is far from being exhaustive since multiple combinations of asperity distributions and charge density distributions can be imagined and computed. The few examples presented illustrate the variety of interaction situations that can be handled by the theoretical formalism described. To our knowledge, the method of calculation outlined in this paper is the first that offers the possibility to concomitantly account for the effects of surface roughness and nonuniform surface charge density. On top of that, various regulation mechanisms as originating from the presence of specific interactions of ions from the background electrolyte with the surfaces can be introduced. The examples in this study clearly highlight the dramatic effects of surface heterogeneities on the Gibbs energy of interaction, both in sign and in magnitude.

We recognize that the surface profile that is generated with the Lego procedure described may be, for certain practical situations, restrictive since the ensuing anisotropy is two-dimensional only. A challenge remains the development of a methodology which allows mimicking of three-dimensional patterns and still accounts for the

chemical and electrical components of the regulation of the double layers at the same level as the 2D analysis presented in this paper.

Appendix

In this appendix, a general expression is given for the electrostatic potential distribution $\psi(x',y')$ in the diffuse part of the double layer at an isolated surface of which the profile is described by the spatial functionality $y' = y_1(x')$ (section A1). (x',y') are the spatial variables and, for mathematical convenience, (x,y) are dimensionless variables (see below). For the sake of simplicity, the constant (surface) potential condition is chosen but the analysis can also be performed for the constant charge case and extended, in a very elegant way, to the situation of interaction between two charged rough surfaces or between charged flat and rough surfaces (section A2). The development proposed constitutes an extension of the work by Tsao,[46] because the Taylor expansion we derive here for $\psi(x,y)$ is valid for smooth as well as moderately rough surfaces (see below).

A1. Solution of the Linearized Poisson−Boltzmann Equation for a Rough Surface: Use of the Perturbation Theory and Calculation of $\kappa^{*-1}(x)$. For a two-dimensional problem, the linearized PB equation with homogeneous dielectric permittivity is written

$$\frac{\partial\psi(x',y')}{\partial x'^2} + \frac{\partial\psi(x',y')}{\partial y'^2} = \kappa^2\psi(x',y') \tag{A1}$$

One can scale the y'-axis and the x'-axis as follows

$$y = \kappa y' \tag{A2}$$

$$x = \kappa x' h_a/l \tag{A3}$$

with h_a the characteristic height of the asperities and l the typical correlation length characterizing the distribution of the protrusions along the surface (see Figure 4B). x and y are from now on dimensionless quantities. Equation A1 is then rewritten

$$\lambda\frac{\partial^2\psi(x,y)}{\partial x^2} + \frac{\partial^2\psi(x,y)}{\partial y^2} = \psi(x,y) \tag{A4}$$

with

$$\lambda = (h_a/l)^2 \tag{A5}$$

Provided that $\lambda < 1$, the potential $\psi(x,y)$ may be expanded as follows

$$\psi(x,y) = \psi_0(x,y) + \sum_{n=1}^{\infty}\psi_n(x,y)\lambda^n \tag{A6}$$

$\psi_0(x,y)$ is the first-order term of the Taylor development and is simply given by

$$\psi_0(x,y) = A_0(x)\exp(-y) \tag{A7}$$

with

$$A_0(x) = \psi^o\exp(y_1(x)) \tag{A8}$$

ψ^o is the surface potential defined by $\psi(x,y = y_1(x)) = \psi^o$, with $y_1(x) = \kappa y_1'(x)$. One can easily show that the terms of order $O(\lambda^n)_{n\geq1}$ are given by the recursive differential equation

$$\frac{\partial^2\psi_n(x,y)}{\partial y^2} - \psi_n(x,y) = -\frac{\partial^2\psi_{n-1}(x,y)}{\partial x^2} \tag{A9}$$

The boundary condition associated with eq A9 is

$$n \geq 1 \qquad \psi_n(x,y = y_1(x)) = 0 \tag{A10}$$

Selecting the solution verifying $\psi(x,y\rightarrow\infty)\rightarrow 0$, the terms ψ_n may be written in the form

$$n \geq 1 \qquad \psi_n(x,y) = (A_n(x) + \sum_{k=1}^{n} B_{k,n}(x)y^k)\exp(-y) \tag{A11}$$

Condition A10 yields the general relationship which exists between the unknown spatial functions $A_n(x)$ and $B_{k,n}(x)$ to be determined

$$A_n(x) = -\sum_{k=1}^{n} B_{k,n}(x)(y_1(x))^k \tag{A12}$$

After substitution of eq A11 in eq A9 and identification of the coefficients $B_{k,n}(x)$ of the polynome in y, one finds the recursion formulas allowing the calculation of the $B_{k,n}(x)$ and, subsequently, of the $A_n(x)$ (eq A12). The mathematical analysis is straightforward but tedious. The results are

$$B_{n,n}(x) = \frac{1}{2^n n!}\frac{\partial^{2n}A_0(x)}{\partial x^{2n}} \tag{A13}$$

$$B_{n-1,n}(x) = \frac{n}{2}B_{n,n}(x) + \sum_{i=1,n\geq4}^{n\text{-}3}\frac{(n-i)!}{2^{i+1}(n-1)!}\frac{\partial^{2i}B_{n-i,n-i}(x)}{\partial x^{2i}} + \frac{1}{2^{n-2}(n-1)!}\frac{\partial^{2(n-2)}B_{1,2}(x)}{\partial x^{2(n-2)}} \tag{A14}$$

$$B_{n-2,n}(x) = \frac{n-1}{2}B_{n-1,n}(x) + \sum_{i=1,n\geq5}^{n\text{-}4}\frac{(n-i-1)!}{2^{i+1}(n-2)!}\frac{\partial^{2i}B_{n-i-1,n-i}(x)}{\partial x^{2i}} + \frac{1}{2^{n-3}(n-2)!}\frac{\partial^{2(n-3)}B_{1,3}(x)}{\partial x^{2(n-3)}} \tag{A15}$$

...

$$B_{n-j,n}(x) = \frac{n-j+1}{2}B_{n-j+1,n}(x) + \sum_{i=1,n\geq j+3}^{n\text{-}j\text{-}2}\frac{(n-i-j+1)!}{2^{i+1}(n-j)!}\frac{\partial^{2i}B_{n-i-j+1,n-i}(x)}{\partial x^{2i}} + \frac{1}{2^{n-j-1}(n-j)!}\frac{\partial^{2(n-j-1)}B_{1,j+1}(x)}{\partial x^{2(n-j-1)}} \tag{A16}$$

...

$$B_{2,n}(x) = \frac{3}{2} B_{3,n}(x) + \frac{1}{2.2!} \frac{\partial^2 B_{1,n-1}(x)}{\partial x^2} \quad \text{(A17)}$$

$$B_{1,n}(x) = B_{2,n}(x) + \frac{1}{2} \frac{\partial^2 A_{n-1}(x)}{\partial x^2} \quad \text{(A18)}$$

For a given λ, calculation of the $A_n(x)$ and $B_{k,n}(x)$ is then iteratively performed up to the order n_o verifying

$$\forall\ (x,y), \quad \psi_{n_o}(x,y)/\psi_{n_o-1}(x,y) \ll 1 \quad \text{(A19)}$$

The potential distribution is then completely determined

$$\psi(x,y) = \psi^o \exp(y_1(x) - y) + \sum_{k=1}^{n_o \geq 1} \sum_{m=1}^{k} B_{m,k}(x)(y^m - [y_1(x)]^m)\lambda^k \exp(-y) \quad \text{(A20)}$$

The dependence of κ^{*-1} (written in its dimensionless form, see eq A2) on the position x is then readily obtained from eq A20

$$\psi^o/e = \psi^o \exp(y_1(x) - \kappa^{*-1}) + \sum_{k=1}^{n_o \geq 1} \sum_{m=1}^{k} B_{m,k}(x)([\kappa^{*-1}]^m - [y_1(x)]^m)\lambda^k \exp(-\kappa^{*-1}) \quad \text{(A21)}$$

A2. Application for the Situation of Interaction between Two Rough Surfaces. We now consider the interaction between two surfaces denoted 1 (left surface) and 2 (right surface) and defined by the profiles $y = y_1(x)$ and $y = y_2(x)$, respectively. As in eq A5, we define λ_1 and λ_2 by

$$\lambda_{1,2} = (h_{a1,2}/l_{1,2})^2 \quad \text{(A22)}$$

with $h_{a1,2}$ and $l_{1,2}$ the characteristic heights and correlation lengths of the asperities on surfaces 1 and 2. We treat the case $\lambda_1 = \lambda_2 = \tilde{\lambda}$. Equations A3−A6 remain valid after replacing λ by $\tilde{\lambda}(<1)$. The first-order term $\psi_0(x,y)$ is written

$$\psi_0(x,y) = C_0(x) \cosh(y) + D_0(x) \sinh(y) \quad \text{(A23)}$$

$C_0(x)$ and $D_0(x)$ are calculated from the boundary conditions $\psi_0(x,y = y_{1,2}(x)) = \psi_{1,2}{}^o$, with $\psi_{1,2}{}^o$ the potential at surfaces 1 and 2. One obtains

$$C_0(x) = \frac{\psi_2{}^o \sinh(y_1) - \psi_1{}^o \sinh(y_2)}{\sinh(y_1 - y_2)} \quad \text{(A24)}$$

$$D_0(x) = \frac{\psi_1{}^o \cosh(y_2) - \psi_2{}^o \cosh(y_1)}{\sinh(y_1 - y_2)} \quad \text{(A25)}$$

The terms $\psi_n(x,y)|_{n\geq 1}$ verify eq A9 and may be written in the general form

$$\psi_n(x,y) = C_n(x) \cosh(y) + D_n(x) \sinh(y) + \sum_{k=1}^{n} E_{k,n}(x) y^k \cosh(y) + \sum_{k=1}^{n} F_{k,n}(x) y^k \sinh(y) \quad \text{(A26)}$$

The functions $C_n(x)$ and $D_n(x)$ are related to the unknown $E_{k,n}(x)$ and $F_{k,n}(x)$ via the conditions $\psi_n(x,y = y_{1,2}(x)) = 0$, which yields

$$C_n(x) = \frac{1}{\sinh(y_1 - y_2)}[\sum_{k=1}^{n} E_{k,n}(x)\{y_1{}^k \sinh(y_2)\cosh(y_1) - y_2{}^k \sinh(y_1)\cosh(y_2)\} + \sinh(y_2)\sinh(y_1) \sum_{k=1}^{n} F_{k,n}(x)\{y_1{}^k - y_2{}^k\}] \quad \text{(A27)}$$

$$D_n(x) = \frac{1}{\sinh(y_2 - y_1)}[\sum_{k=1}^{n} F_{k,n}(x)\{y_1{}^k \sinh(y_1)\cosh(y_2) - y_2{}^k \sinh(y_2)\cosh(y_1)\} + \cosh(y_2)\cosh(y_1) \sum_{k=1}^{n} E_{k,n}(x)\{y_1{}^k - y_2{}^k\}] \quad \text{(A28)}$$

To obtain the $E_{k,n}(x)$ and $F_{k,n}(x)$, one can rewrite the expression A26 for the potential in terms of $\exp(y)$ and $\exp(-y)$ so as to return to a treatment similar to the one presented in section A1. One then easily shows that the recursion formulas (A13−A18) allow computation of the $E_{k,n}(x)$ and $F_{k,n}(x)$ via the simple transformations

$$B_{k,n}(x) \equiv \frac{1}{2}(E_{k,n}(x) - F_{k,n}(x)) \quad \text{(A29a)}$$

$$A_n(x) \equiv C_n(x) - D_n(x) \quad \text{(A29b)}$$

$$y \equiv -y \quad \text{(A30a)}$$

$$B_{k,n}(x) \equiv \frac{1}{2}(E_{k,n}(x) + F_{k,n}(x)) \quad \text{(A30b)}$$

$$A_n(x) \equiv C_n(x) + D_n(x) \quad \text{(A30c)}$$

The potential distribution (eq A26) is found after solving the system of eqs (A24-A25, A27−A30) up to the order n_o verifying A19.

LA030404F